RESEARCH ARTICLE

Macromolecular Materials and Engineering
Open Access
www.mame-journal.de

Tailoring Nanostructured Cellulose for Efficient Pickering Emulsions Stabilization

Annachiara Pirozzi, Paolo Bettotti, Tiziano Facchinelli, Elvira D'Amato, Marina Scarpa, and Francesco Donsì*

Nanostructured celluloses, nanofibrils (CNFs) and nanocrystals (CNCs), are prepared through TEMPO-mediated oxidation by controlling the intensity of the process modulated by catalyst concentration and processing time. These nanomaterials are evaluated as stabilizers for Pickering emulsions, fabricated using high-pressure homogenization (HPH). Both CNFs and CNCs exhibit efficient steric and electrostatic stabilization of oil-in-water (O/W) emulsions. CNFs display strong inter-droplet interactions, leading to the formation of a 3D fibrous network emulsion with higher viscosity compared to CNCs-stabilized emulsions. However, CNFs also show a higher tendency toward flocculation, due to fibrils' entanglement in the continuous phase. Interestingly, the HPH treatment has a notable impact on the CNFs' interfacial layer, enhancing the emulsifying ability of CNFs and improving stability against coalescence. Conversely, CNCs-stabilized emulsions exhibit lower viscosity but demonstrate higher interfacial activity and stabilization capability. Remarkably, no phase separation during 10 months of refrigerated storage, indicating excellent long-term stability. Importantly, the HPH treatment does not significantly change the emulsifying ability of CNCs. In conclusion, this study highlights the possibility of obtaining nanocelluloses (NCs) with tailored emulsifying properties by regulating the intensity of TEMPO-mediated oxidation applied to pulp cellulose. These findings open up new opportunities for the development of innovative ingredients for the food and cosmetic industries.

1. Introduction

Emulsion systems have undergone thorough investigation with respect to their complex interactions with product interfaces and other ingredients, alongside a comprehensive examination of stabilization issues.[1] These investigations have revealed a broad spectrum of applications across various industries, including agri-food, biomedical, petrochemistry, and environmental remediation. In recent years, there has been a shift in wards smaller scales, particularly microemulsions and nanoemulsions, characterized by droplet sizes <1 µm. To stabilize these emulsions without relying on surfactants, there has been growing interest in utilizing particles as stabilizers at the oil–water interface.[2,3] Pickering emulsions, stabilized by particles, offer several advantages,[4] such as reduced environmental and health concerns and enhanced stability due to the nearly irreversible absorption of the particles at the liquid interface,[5] where they form a compact and dense layer, leading to efficient steric repulsion.[6] These emulsions hold significant promise in the pharmaceutical and food industries for applications like drug delivery systems, nutraceutical vehicles, edible films, and wastewater management.[7–10] However, despite the recognition of the vast potential of Pickering emulsions, their practical implementation requires further investigation. The characteristics of particles employed as stabilizers play a fundamental role[3] in their behavior at the oil-water interface, influencing self-assembling tendencies, interfacial particle layer thickness, and cohesion. In addition to the chemical composition and surface functional groups, physical parameters, such as size, shape, and crystallinity, impact the tuning of Pickering emulsion characteristics and performance according to the desired application.[11]

While numerous solid particle materials of both inorganic or organic origins have been employed,[12] recent interest has turned to nanoparticles from natural sources, as they offer the advantage of self-assembling driven by nanoscale forces[13] coupled with limited environmental impact and no toxicity concerns.[14] Within this context, various organic particles of natural origin have been explored, including biopolymers such as

A. Pirozzi, F. Donsì
Department of Industrial Engineering
University of Salerno
via Giovanni Paolo II 132, Fisciano 84084, Italy
E-mail: apirozzi@unisa.it
P. Bettotti, T. Facchinelli, E. D'Amato, M. Scarpa
Department of Physics
University of Trento
via Sommarive 14, Povo, Trento 38123, Italy

The ORCID identification number(s) for the author(s) of this article can be found under https://doi.org/10.1002/mame.202300451

DOI: 10.1002/mame.202300451

polysaccharides, lignin, and proteins, as well as microorganisms and molecular assemblies. However, it is noteworthy that only a few of these natural particles have demonstrated the capability to stabilize Pickering emulsions in their pristine state. In the majority of cases, a modification process was necessary to impart the required techno-functional properties for effective emulsion stabilization.[15] The need for such modifications underscores the importance of tailoring the particle characteristics to achieve optimal performance as Pickering emulsion stabilizers.

Cellulose-derived nanomaterials, known as NCs, have emerged as promising stabilizers due to their abundance, sustainability, environmental friendliness, and biocompatibility.[16,17] While NCs in pristine state, find use in films, hydrogels,[18] and emulsions[19] fabrication, chemical modifications and hybridizations with inorganic nanoparticles enhance their versatility for various applications.[20–24]

NCs exhibit good water dispersibility, leading to highly stable colloidal suspensions. Their amphiphilic nature arises from the exposure of crystalline faces with largely different polarity, making them particularly appealing for the stabilization of water-oil interfaces, such as for Pickering emulsion[25–27] and capillary suspensions.[28] Among different methods developed for obtaining NCs from various sources,[29] TEMPO-mediated oxidation stands out as the most versatile approach.[30] This method allows for the generation of NCs with diverse morphologies (NCs particles with 10–30 nm in diameter and 40–60 nm in length) by fine-tuning the reaction conditions.[31] The ability to control NCs' morphology through TEMPO-mediated oxidation makes it an indispensable tool for tailoring NCs' properties to suit specific applications, despite the high carbon emissions and generation of waste streams associated with the process.[32] Consequently, there is a growing interest in developing milder reaction conditions that can offer a more sustainable and eco-friendly alternative.[33]

Among NCs, CNFs and CNCs have drawn attention for their high and low aspect ratios, respectively. The diameter of CNFs is typically reported to be in the nanoscale, i.e., ≈1–100 nm and their length is typically up to a few micrometers. Conversely, CNCs' diameter and length are in the range of 2–25 nm and 100–750 nm, respectively.[34] These rather wide and overlapping ranges do not allow a clear distinction between CNCs and CNFs based on their size. Therefore, while previous research has mainly focused on their size-based distinction, recent trends base the classification on their unique structural properties, such as flexibility and stiffness, which play a crucial role in their emulsification behavior.[35] More specifically, CNCs are characterized by being stiffer and shorter rods, while CNFs are longer and more flexible, with kinks and splits leading to entanglement.[35] Moreover, exploring the structural variations of these nanomaterials while maintaining their similar chemical nature presents a fascinating opportunity. Numerous studies have explored correlations between NCs length,[36–38] preparation method, chemical modification,[39,40] and the strength and stability of emulsion structure and droplet size. These investigations have been the subject of recent reviews,[26] providing valuable insights into the relationship between NCs properties and their emulsification performance.

Despite the potential of NCs as Pickering emulsion stabilizers, systematic investigations into the fundamental aspects governing their stabilizing performance are limited.[41] This limitation is attributed to the vast number of experimental parameters that need consideration in NCs fabrication, hindering a comprehensive understanding of the correlation between NCs properties and emulsion characteristics. For example, in our recent study, we investigated the emulsification ability and emulsion stabilization capability of NCs derived from mechanical processing of pulp cellulose, using ball milling and HPH.[42] While the results showed promise regarding Pickering emulsion stabilization, the lack of precise control over the mechanical processes resulted in wide size distributions (with the 50th percentile of the cumulative size distribution of ≈16 µm for ball milling and 22 µm for HPH) and varying structures (amorphous for ball milling and defibrillated for HPH). As a consequence, drawing general conclusions regarding the relationship between NCs' structure and function in this context proved challenging.

Therefore, in this study, we address the challenge of advancing the understanding of the correlation between NCs structure and techno-functional properties related to emulsification, by employing the well-consolidated TEMPO-mediated oxidation, followed by ultrasound-assisted dispersion, to prepare NCs in the form of small and flexible fibrils (CNFs) and rod-like crystals (CNCs), with controlled morphology and surface charge. The objective is to establish a correlation between the physicochemical properties of CNFs and CNCs and the resulting Pickering emulsion properties (ζ-potential, microstructure, and rheological properties) to enhance emulsion behavior and stability over time. By providing insights into the interplay between NCs characteristics and emulsion performance, our work contributes to advancing the utilization of NCs in various applications requiring stable emulsions.

2. Results and Discussion

2.1. Morphology and Interfacial Properties of NCs

Two types of NCs, CNCs and CNFs, obtained from different treatment conditions of the same cellulose raw material, were used as stabilizers for Pickering emulsions.

The morphological, topological, and size features of the as-prepared CNCs and CNFs were assessed using AFM. **Figure 1** displays representative images of CNCs and CNFs, with CNCs characterized by a needle-like structure, and CNFs by a fibrous network. Statistical analysis of CNCs' size, based on a data set of 900 CNCs images, individually resolved from AFM, indicated a length of 170 ± 90 nm and a cross section of 3.0 ± 0.5 nm. For CNFs, a comprehensive statistical analysis of size was challenging due to the entanglement propensity of the flexible and disordered regions within the fibers, as evident in the AFM images. However, an estimated average fiber cross section of 5 nm and a length >1 µm were observed.

FT-IR spectroscopy was used to analyze the functional groups present in the NC samples. **Figure 2** illustrates representative spectra of CNCs (black trace) and CNFs (red trace). These spectra exhibit typical features characteristic of NCs. Specifically, notable peaks include the C—H rocking at 910 cm^{-1}, C—O bond vibrations spanning in the range 1030–1100 cm^{-1}, the antisymmetric stretching vibration of the C—O—C glycosidic bond at 1160 cm^{-1}, stretching vibration of the C—H bond at 2900 cm^{-1}

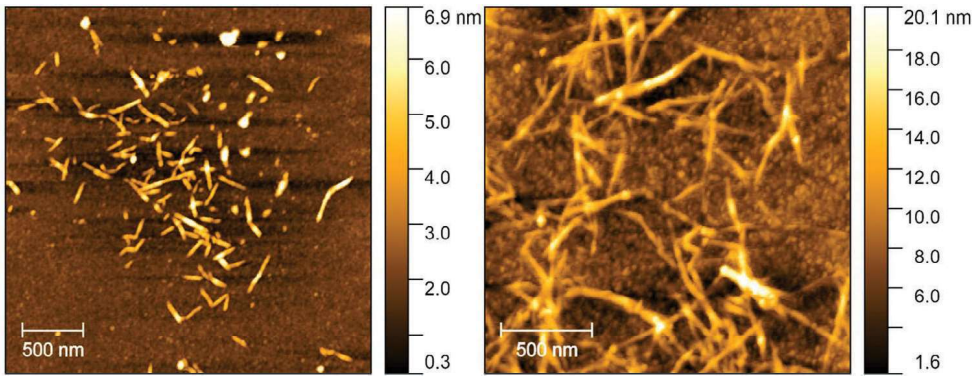

Figure 1. AFM images of CNCs (left panel) and CNFs (right panel).

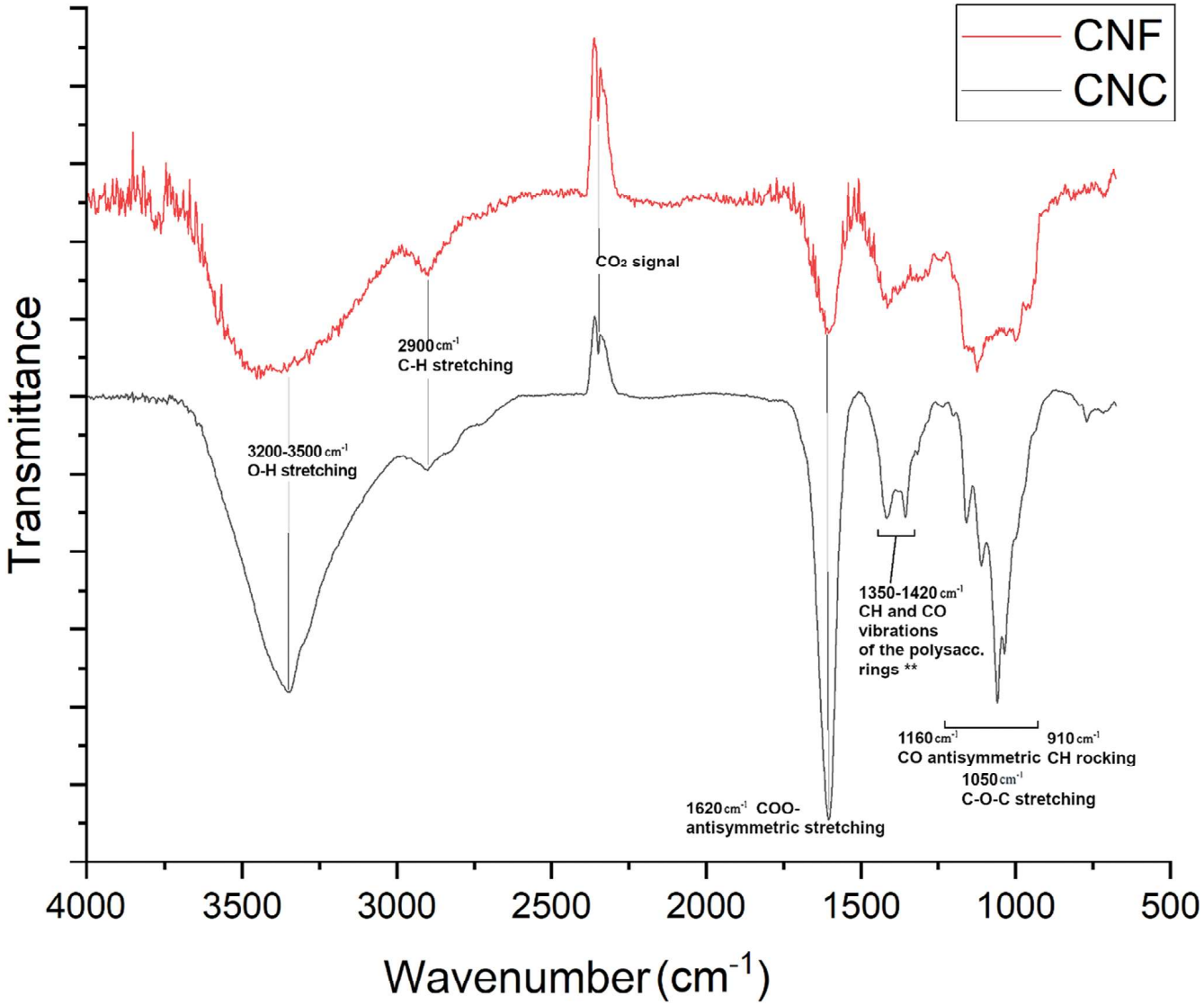

Figure 2. FT-IR spectra of CNCs (black trace) and CNFs (red trace). The spectra were normalized to the intensity of the peak at 2900 cm^{-1}, taken as internal reference.

Figure 3. Suspensions of CNCs (on the left) and CNFs (on the right).

and a broad band corresponding to the stretching vibrations of the O—H bonds of primary and secondary hydroxyl groups within the range 3200–3500 cm^{-1}.[43]

A prominent peak at 1620 cm^{-1} indicates the presence of carboxylates introduced by the TEMPO-mediated oxidation. The varying degrees of oxidation of CNCs and CNFs become apparent when comparing the intensities of the carboxylate peaks in the spectra of Figure 2, normalized to the peak at 2900 cm^{-1}, which remains unaffected by the TEMPO-mediated reaction. The normalized spectra reveal a more substantial oxidation of CNCs compared to CNFs, aligning with the milder oxidation conditions used to produce larger sizes and preserve some amorphous regions within CNFs.

The FT-IR findings were confirmed by conductometric titrations, yielding degree of oxidation values of 0.6 ± 0.2 μmol mg^{-1} and 1.4 ± 0.1 μmol mg^{-1} for CNFs and CNCs, respectively.

The aqueous suspensions of CNCs and CNFs, as depicted in **Figure 3**, were evaluated for their physical properties, including the average hydrated size, polydispersity, electrophoretic mobility, and average cross section obtained from AFM images. The summarized results are reported in **Table 1**.

DLS data revealed an average hydrodynamic size of 652 nm (polydispersity 24.4) and 163 nm (polydispersity 23.3) for CNFs and CNCs, respectively. Notably, high ζ-potential values, specifically −47.0 ± 2 mV and −37 ± 2 mV at pH 6.0 for CNCs and

Table 1. Morphological characteristics of CNCs and CNFs before and after HPH processing.

Sample	Hydrated size[a] [nm]	Polidispersity[a]	ζ-potential[a,b] [mV]	Cross section[c] [nm]
CNCs	170	23.3	−46 ± 3	3.0 ± 0.5
CNFs	652	24.4	−35 ± 2	4.9 ± 0.5
CNCs after HPH	155	26.1	−47 ± 2	4.1 ± 0.5
CNFs after HPH	325	37.7	−30 ± 2	5.0 ± 0.5

[a] The measurements were conducted using a DLS apparatus; [b] The values were obtained from electrophoretic mobility in aqueous solution; [c] The cross-section was determined through a statistical analysis of AFM images, utilizing a data set of 900 data samples for the as-prepared CNCs and CNFs and 100 samples for HPH-treated CNCs and CNFs.

CNFs, respectively (Table 1), underscore the presence of substantial interparticle electrostatic repulsion forces, crucial for colloidal stabilization.[44] These findings suggest that CNCs and CNFs share a similar chemical composition, differing primarily in the content of carboxylate groups.

The observed cross-section value for CNCs (3.5 nm) aligns with existing literature data. Conversely, CNFs tend to aggregate into macrofibrils, and the average cross-section typically falls within the range of 18 and 20 nm, decreasing to 7–8 nm when the CNFs surface is highly charged.[45] An average value of 5 nm indicates effective defibrillation through ultrasounds.

The distinct length and shape of the NCs used in this study are evident: CNCs exhibit a needle-shaped structure, whereas CNFs appear elongated and partly disordered. Finally, both NCs preparations form stable dispersions, making them promising candidates for Pickering emulsion stabilization.

The wettability of solid particles on oil surfaces is an important factor to stabilize the oil emulsion particles through the adsorption of solid particles on oil surfaces.[40] Therefore, the impact of CNCs and CNFs on interfacial phenomena was explored by tracking the change of interfacial tension at the water-oil interface. **Figure 4** illustrates the dynamic adsorption behavior of CNCs and CNFs at the water-oil interface, investigated by monitoring the change in interfacial tension (γ) with adsorption time (0–2500 s) at 25 °C. Upon the addition of both CNCs and CNFs to deionized water, a significant reduction in the interfacial tension of the oil-water interface was observed. Notably, CNFs exhibited a higher reduction than CNCs, suggesting a more pronounced dynamic adsorption behavior and the strong binding of particles to the interface. Once adsorbed, a greater number of CNFs nanoparticles may be able to orient themselves in the interface, given the increased flexibility of the molecules, and prevent droplet coalescence compared to typical molecular surfactants in the emulsion stabilization.[40] The interfacial tension of water rapidly decreased within the initial 500 s, due to the adsorption of more hydrophilic oil components, eventually reaching a gradual equilibrium. Over time, both CNCs and CNFs demonstrated a decrease in interfacial tension, converging toward equilibrium values (γ_∞). These equilibrium values, estimated using an exponential decay model (Equation 2), were determined to be 16.7 and 13.8 mN m^{-1} for CNCs and CNFs, respectively.

The γ_∞ value for CNCs was slightly lower than that estimated for pure water (19.2 mN m^{-1}), indicating a reduced ability of

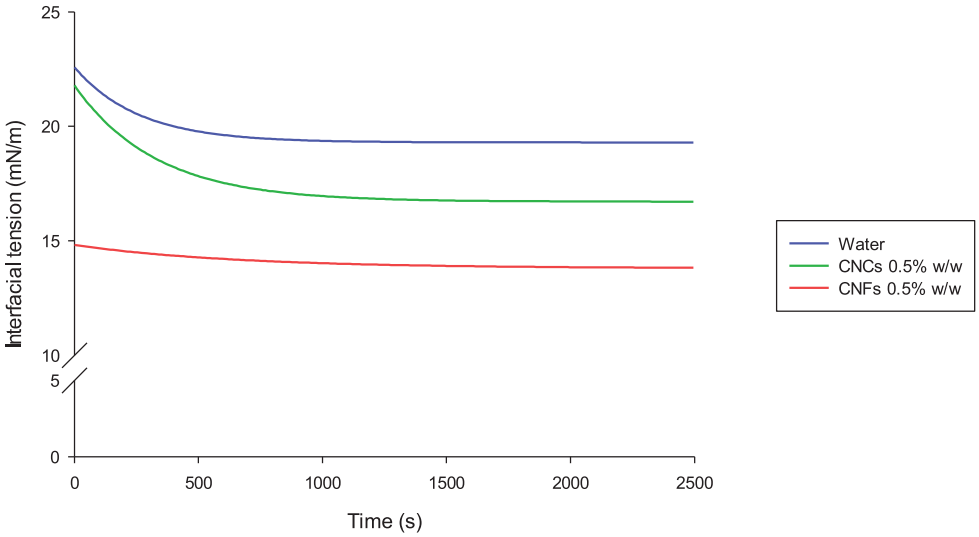

Figure 4. Peanut oil-water interfacial tension for pure water (—), aqueous suspensions at 0.5 wt% CNCs (—), and 0.5 wt% CNFs (—).

CNCs particles to interact with the oil-water interface. In contrast, CNFs nanoparticles with the lowest interfacial tension corresponded to the maximum number of adsorbed at the water-oil interface, effectively reducing its free energy. This suggests, based on interfacial tension measurements, that CNFs have the potential to be more effective in emulsifying oil and water by adsorbing on the surfaces of oil droplets with high desorption energies, making the O/W Pickering emulsions thermodynamically more stable.[46] Moreover, the dense structure network of CNFs and their entangled nature plays a significant role in emulsions' physical properties, leading to act more as a rheological modifier in the continuous water phase than as a Pickering stabilizer.[47] It is crucial to consider the effectiveness of emulsifiers in terms of rapidly reducing interfacial tension, strong binding to the interface, and protection against droplet flocculation or coalescence. The interfacial tension values of ionic surfactants, i.e., Tween 20 and Tween 80, and of β-cyclodextrin, commonly used as emulsifiers or stabilizers, have been estimated to be ≈35–40 mN m^{-1}[48] and 20 mN m^{-1},[49] respectively. The higher interfacial tension values for ionic surfactants and β-cyclodextrin oligosaccharide suggest lower adsorption at the oil–water interface compared to NCs particles, providing insights into the potential of CNCs and CNFs as stabilizers.

The protocol for stabilizing Pickering emulsion (elaborated details provided later) involves HPH processing at 80 MPa, following the methodology outlined by Pirozzi et al.[42] It is worth noting that this treatment could not only impact droplet size but also potentially influence the physical properties of individual NCs' particles. The disruptive energy from HPH induces a dynamic assembly-disaggregation process of the droplets.

Previous studies indicate that HPH processing can effectively reduce the particle length of NCs without altering their functional groups.[36] Considering this, the physical characterization of both nanoparticles, CNCs and CNFs, has been conducted after subjecting their aqueous suspensions to HPH processing. The AFM images of HPH-treated NCs are presented in **Figure 5**, and physical parameters are detailed in Table 1. These investigations provide insights into the changes induced by HPH on the NCs and enable an assessment of its potential impact on emulsion stabilization.

The results outlined in Table 1, along with the comparison between Figures 1 and 5, suggest that HPH treatment has a

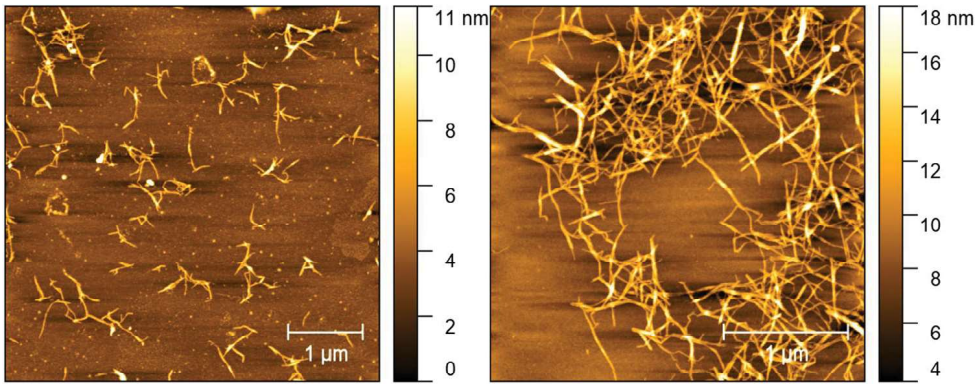

Figure 5. AFM images of CNCs (left panel) and CNFs (right panel) after HPH processing at 80 MPa.

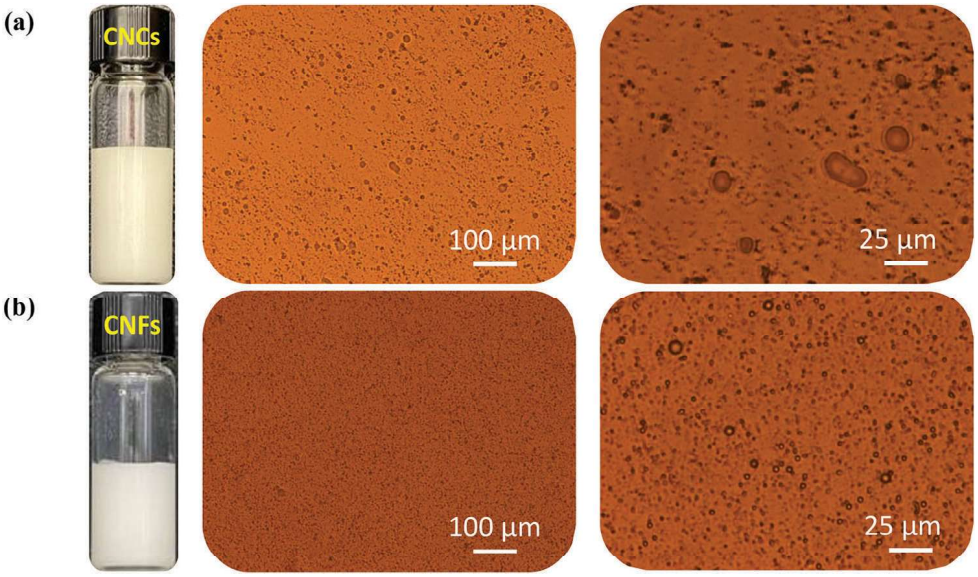

Figure 6. Visual observation and micrographs of Pickering emulsion stabilized with a) CNCs and b) CNFs at two different magnifications (10× on the left-hand side and 40× on the right-hand side).

negligible impact on the size of rod-like CNCs and their electrical interface properties. Conversely, the length of CNFs consistently decreases following HPH treatment. The average hydrated size of CNFs is nearly halved, while the cross-section remains unaffected. The characteristic bending propensity inherent to fibrous nanostructures is still evident in the right panel of Figure 5. Post-HPH treatment, the aspect ratio for CNFs is estimated to be greater than 100, while for CNCs, it is approximately 54. These findings highlight the differential effects of HPH shear and impact forces (elongation, hydrodynamic cavitation, turbulence, and pressure gradient)[50] on the two types of NCs and emphasize potential implications for their utilization in Pickering emulsions stabilization. Specifically, CNCs can effectively interact at the oil-water interface and form a robust particle network, thereby enhancing emulsion stability and preventing coalescence and Ostwald ripening, as HPH treatment does not significantly alter their shape and properties. Conversely, HPH causes significant physical changes in CNFs particles, such as breakage of inner bonds (fibrillation) and shortening of the fibers,[51] while preserving their properties. The improved fibrillation and the reduction of fiber length makes the fiber more flexible, reducing the bending stiffness of the fiber wall. Shorter CNFs with improved dispersion are a desired effect to improve the efficient formation of a dense and stable particle network at the emulsion interface. Therefore, based on the revealed results, the CNFs particles subjected to HPH treatment during the formation of Pickering emulsions hold great significance for the stabilization effect, preventing droplet aggregation and improving long-term emulsion stability. Remarkably, the size and morphology of NCs are a critical factor indicating emulsifying activity and stability, as well as their applications. Based on the results discussed above, the following two points are proposed for NCs-stabilized Pickering emulsions' mechanisms: i) CNCs stabilize O/W emulsions by forming a dense layer at the oil droplet surface, as well as between adjacent oil droplets, due to their nanosize and highly negative ζ-potential already before the HPH treatment, and ii) CNFs stabilize O/W emulsions by forming a layer of entangled fibrils network at oil droplet surfaces, due to size halved and the defibrillation degree after the HPH treatment.

2.2. Characterization of NCs-Stabilized Pickering Emulsions

The formation, morphology, and time behavior of Pickering emulsions stabilized with CNCs and CNFs were examined through optical imaging, while the emulsions size distributions were measured using laser diffraction.

Figure 6 shows the microstructure of freshly prepared Pickering emulsions stabilized with CNCs (Figure 6a) and CNFs (Figure 6b) at a 5 wt% oil phase. In both cases, oil droplets of relatively uniform size were observed, with CNFs-stabilized Pickering emulsion exhibiting a better-textured overall structure. The oil droplets in CNFs-stabilized emulsions displayed a spherical structure with a uniform size of ≈3 µm. CNCs-stabilized emulsions are still uniform in size; however, it is likely that a fraction of CNCs particles remain partially dispersed in water, as suggested by Bertsh and Fisher.[52] These authors demonstrated that CNCs at the fluid interphase tend to be almost fully submerged in the water phase due to their low desorption energy from the interphase, and hence show a dynamic adsorption/desorption behavior. Conversely, nanofibrillated CNFs, coupled with the thickening effect of the residual short amorphous tract, facilitated more efficient entrapment of oil droplets, resulting in the development of a 3D emulsified structure. It can be speculated that the enhanced entanglement capacity facilitated the bridging of neighboring droplets, creating an interconnected droplet-CNFs fiber 3D network. Overall, the micrographs in Figure 6 are in agreement with previous observations in the preparation of Pickering emulsions stabilized by CNFs.[42]

Remarkably, despite the reported differences in interfacial tension and ζ-potential, both CNCs and CNFs displayed outstanding stability against droplet coalescence, with no observed phase sep-

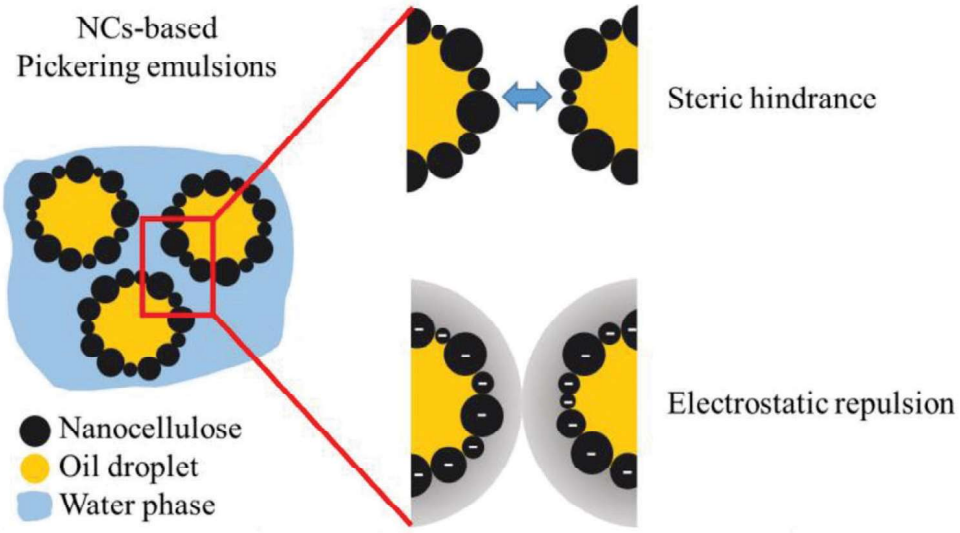

Figure 7. Electrostatic stabilization interactions of CNCs- and CNFs-based Pickering emulsions.

aration during refrigerated storage at 4 °C. This remarkable stability is likely attributed to the effective strong repulsive forces (steric hindrance and electrostatic repulsion stabilization mechanisms) provided by both CNCs and CNFs that inhibit droplet aggregation, ensuring the long-term integrity and functionality of the Pickering emulsions (**Figure 7**).

The impact of the emulsion processing in this study was investigated in terms of droplet size distribution (**Figure 8**) and mean droplet diameters (**Table 2**) for both the coarse emulsions (after high-shear mixing (HSM)) and the final emulsions (after HPH treatment). The measured size distributions align with the micrographs in Figure 6, indicating a significant effect of the process intensity on size distribution.

Notably, the droplet characteristic diameters and the distribution span exhibited a sharp decrease after the application of HPH treatment. The particle size distribution of emulsions treated by HSM was multimodal, with three peaks (CNCs) and two peaks (CNFs) in the distribution curve within a range from 1 to 100 µm. In contrast, after HPH treatment, the volume fraction of small droplets increased, resulting in monomodal and narrow droplet size distribution with span values of 1.2 and 1.4, and d(0.9) values of 2.23 and 2.92 µm for CNCs and CNFs, respectively. Similarly, d(0.1) value was reduced to sub-micrometric size range, and d(0.5) to the micrometric size range for both HPH emulsions. The volume mean diameters D[4,3] were in the range of 1.4–1.8 µm, and the surface mean diameters D[3,2] in the range of 1.2–1.4 µm (Table 2). Low D[3,2] values are generally associated with higher kinetic stability due to the reduction of the effects of gravitational phase separation, as the droplet separation velocity is proportional to their square radius.[53] Moreover, the droplet size, influenced by the application of HPH mechanical treatment, is known to have an important impact on the rheology of emulsions[42] and, as a consequence, to play a crucial role in controlling the physical properties of emulsions for food, cosmetics, and various industrial applications. Fine emulsions with decreased droplet size and span values have much higher viscosities and storage moduli than the corresponding coarse emulsions, as found by Pal.[54] This phenomenon could be ascribed to different reasons: i) the mean distance of separation between the droplets decreases with the decrease in droplet size, leading to an increase in hydrodynamic interaction and viscosity; ii) the effective dispersed-phase concentration increases; and iii) the width of the particle size distribution decreases.

NCs are expected to stabilize the Pickering emulsions through two primary mechanisms, as schematic represented in **Figure 9**: i) stabilization via the formation of interfacial film/envelopes of particles surrounding oil droplets of the dispersed phase, that prevents them from coalescing; and ii) encapsulation of the oil droplets in a 3D network[26] of aggregated nanoparticles, that inhibits their movement.

The extent of surface coverage plays a pivotal role in Pickering stabilization, governed by the interfacial properties of the NCs. To explore this aspect, the relationship between emulsion size and the volume fraction of the dispersed phase (i.e., oil) was investigated and the emulsion coverage, defined as the maximum number of NCs entrapped at the droplet, interface, was estimated. Interestingly, the percentage coverage of emulsions stabilized with different types of NCs, after HPH processing, exceeded 100% (377% and 131% for CNCs and CNFs, respectively). This result confirms that NCs create an efficient interfacial coating, with a denser arrangement observed for CNCs. This finding is in line with the observations of Kalashnikova et al.[55] who suggested that the higher steric hindrance of longer CNCs limits denser packing at the interface, leading to porous multilayered profiles. The strong interaction observed between the cellulosic nanostructure and the oil droplets, as indicated by the present data, plays a crucial role in enhancing the physical stability of the Pickering emulsions. This interaction can contribute to various stabilization mechanisms, including i) increasing the viscosity of the continuous phase, ii) reducing the emulsion droplets size, and/or iii) minimizing the difference in density between the continuous phase and the dispersed one.[55–59] To further under-

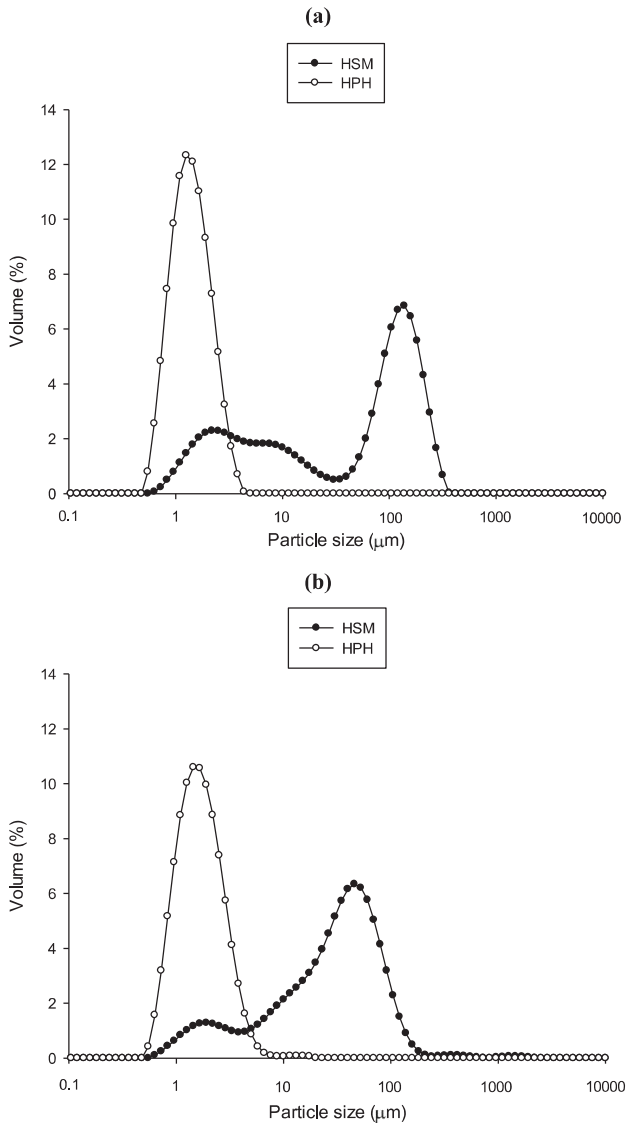

Figure 8. Droplet size distribution of the O/W Pickering emulsions stabilized by CNCs (a) and CNFs (b) homogenized by HSM (—●—) or HPH treatment (—○—).

stand the impact of the morphological properties of NCs on the viscosity of the emulsions and its relation to stability, rheological properties of the emulsions were evaluated. The Pickering emulsions stabilized by CNCs and CNFs exhibited typical shear-thinning behavior, wherein the apparent viscosity decreased with increasing shear rate. Specifically, for CNFs, this behavior was observed across the entire shear rate range of 0.1 to 100 s^{-1}, while for CNCs, a plateau was reached at shear rates higher than 1 s^{-1}. This behavior is linked to the structural deformation of the emulsion, with the breakdown of entangled 3D networks and orientation along flow lines occurring more easily for CNCs emulsions (**Figure 10**).[60,61] Moreover, CNFs contributed to increased emulsion apparent viscosity values[62] compared to an equivalent amount (mg mL^{-1}) of CNCs, likely due to their greater flexibility and defibrillation, allowing the formation of internal entanglements in the continuous phase. These entanglements, combined with the Van der Waals- or hydrogen bond-mediated fiber-to-fiber interactions, restrict the movement of the oil droplets and enhance emulsion stability.

Table 2. Particle size distribution (expressed as characteristic diameters and span) of Pickering emulsions homogenized by HSM or HPH treatment and stabilized by CNCs and CNFs.

	O/W Pickering emulsion stabilized by CNCs		O/W Pickering emulsion stabilized by CNFs	
	HSM	HPH	HSM	HPH
d(0.1) [μm]	2	1	3	1
d(0.5) [μm]	70	1	30	2
d(0.9) [μm]	180	2	79	3
D[4,3] [μm]	77	1	42	2
D[3,2] [μm]	6	1	8	1
Span (−)	3	1	3	1

2.3. Stability of NCs-Stabilized Pickering Emulsions

Emulsifying activity and emulsion stability, evaluated through EAI and ESI values, respectively, are recognized as crucial parameters for assessing the emulsifier's efficacy in forming a stable emulsion. EAI and ESI values, presented in **Table 3**, are greatly influenced by the hydrophobicity and ionic charge of CNCs and CNFs. A significantly ($p < 0.05$) higher value of interfacial area stabilized per unit of weight (EAI = 186 ± 4 m^2 g^{-1}) was observed for CNCs compared to CNFs, likely attributed to the smaller molecules of CNCs, facilitating quicker diffusion and adsorption onto the oil–water interface.[63,64]

This behavior can be explained in terms of the observed differences in interfacial tension (14 and 19 mN m^{-1} for CNFs CNCs, respectively, at 2000 s), which are expected to influence emulsifying performance. This includes their ability to interact with the oil–water interface and facilitate droplet formation, while the high surface charge density enhances droplet stability through electrostatic repulsion.[56]

Simultaneously, ESI was found to be 0.14 ± 0.03% and 0.33 ± 0.09% for CNCs and CNFs-stabilized emulsions, respectively. The higher ESI observed for CNFs-stabilized emulsion significantly differed ($p < 0.05$) from that stabilized with CNCs, likely due to the greater molecular flexibility of CNFs, a crucial factor in forming a compact interfacial layer and promoting emulsion stability.

Remarkably, the results in Table 3 show that the effect of HPH was more pronounced for CNFs-stabilized emulsions than for CNCs-stabilized ones: EAI values increased tenfold for the former and only doubled for the latter upon HPH processing, aligning with the morphological data discussed earlier. Therefore, thanks to HPH treatment, the emulsification ability (EAI) of CNFs becomes comparable to that of CNCs. The capability to stabilize emulsions (ESI) was higher in CNFs-stabilized emulsions, primarily due to the higher viscosity of the continuous phase, which slowed down gravitational separation phenomena.

To assess the long-term stability of various types of NCs in Pickering emulsions, changes in microstructure and mean droplet diameter were monitored over a 10-month period at 5 °C.

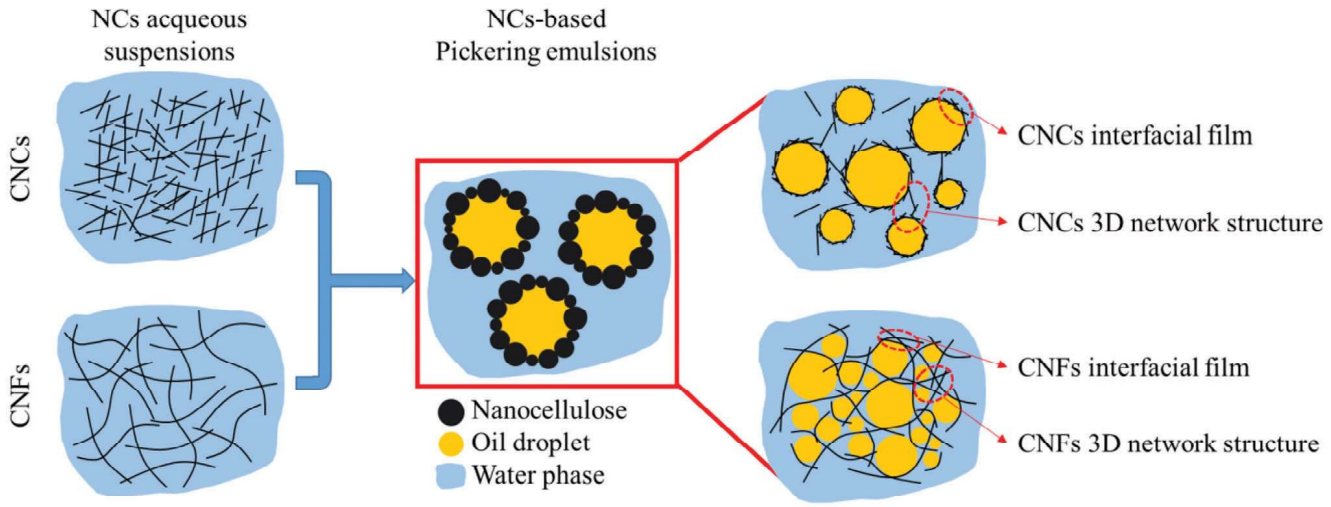

Figure 9. Schematic illustration of stabilization mechanisms of CNCs- and CNFs-based Pickering emulsions.

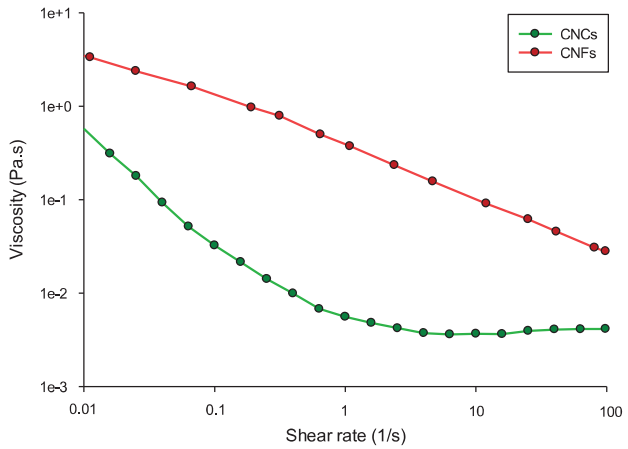

Figure 10. Rheological properties of emulsions prepared by HPH and stabilized by CNCs (—●—) and CNFs (—●—).

Figure 12 presents microscope images of emulsions stabilized by CNCs and CNFs. Visual observations show that CNCs efficiently stabilized Pickering emulsions, without exhibiting signs of precipitation or flocculation throughout the entire storage period.

Table 3. Emulsifying activity (EAI) and emulsion stability (ESI) parameters of Pickering emulsions homogenized by HSM or HPH treatment and stabilized by CNCs and CNFs.

	O/W Pickering emulsion stabilized by CNCs		O/W Pickering emulsion stabilized by CNFs	
	HSM	HPH	HSM	HPH
EAI [m^2 g^{-1}]	89.49 ± 6.60^b	186.03 ± 4.40^d	16.60 ± 1.54^a	150.02 ± 2.98^c
ESI [%]	0.05 ± 0.01^a	0.14 ± 0.03^a	0.15 ± 0.03^a	0.33 ± 0.09^b

Different letters denote significant differences ($p < 0.05$) among the different samples within each row ($n = 3$).

The appearance of CNCs-stabilized emulsion indicated no phase separation after 10 months.

Interestingly, after 10-month of storage, the mean droplet diameter of the emulsions decreased compared to the freshly prepared samples (Figure 12), indicating an unusual phenomenon, contrary to the coalescence of the particles, which could instead be expected during emulsion extended storage. This behavior can presumably be attributed to different mechanisms[65]: i) the strong electrostatic repulsion due to the high surface potential of the CNCs-coated oil droplets (ζ-potential of −46 mV (Table 1)); ii) the strong steric repulsion due to the rearrangement of CNCs layers around the droplets' surfaces, forming a network structure that effectively prevents oil droplets from coalescing into larger droplets during the emulsion aging process[66]; and iii) the irreversible adsorption of the CNCs at the oil droplet surfaces based on the Pickering stabilization.

In contrast, flocculation of the emulsions prepared with CNFs is evident at the end of the storage period, with the formation of aggregates visible to the naked eye and under optical microscopy (**Figure 11**). Generally, smaller particles stabilizing the water-oil interface require less energy for removal. In the present case, lower stability is associated with larger particles, possibly due to the bridging flocculation of CNFs, aligning with the observed increase in CNFs-based emulsion viscosity due to fiber entanglements in the continuous phase.

The formation of aggregates is also evident from the particle size distribution data in **Figure 12**, possibly arising from CNFs chain interactions leading to droplet flocculation through a particle bridging mechanism at water–oil interface. Moreover, the EAI and ESI values of the emulsions were determined after 10 months of storage. Emulsions, post-storage period, exhibited lower EAI values than those freshly prepared (54.27 ± 4.02 m^2 g^{-1} and 45.23 ± 4.16 m^2 g^{-1} for CNCs and CNFs, respectively), but constant ESI values (017 ± 0.10% and 0.32 ± 0.02% for CNCs and CNFs, respectively).

In addition to assessing the 10 months of storage, the influence of the external environmental stimuli, i.e., temperature, ionic strength, and pH on the physical stability of the Pickering

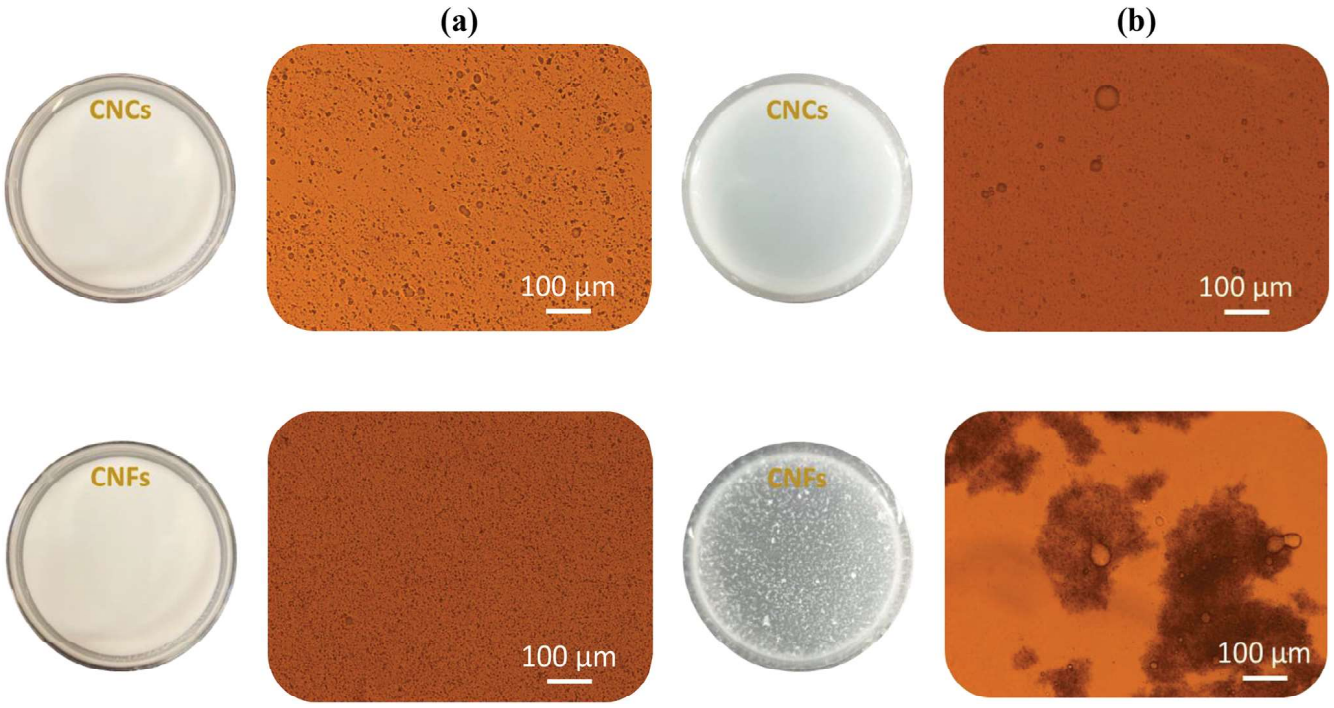

Figure 11. Visual observation and micrographs of (a) freshly prepared Pickering emulsions and (b) emulsions after 10-months of storage at 5 °C (10× of magnification) stabilized by CNCs and CNFs are presented in the first and second rows, respectively.

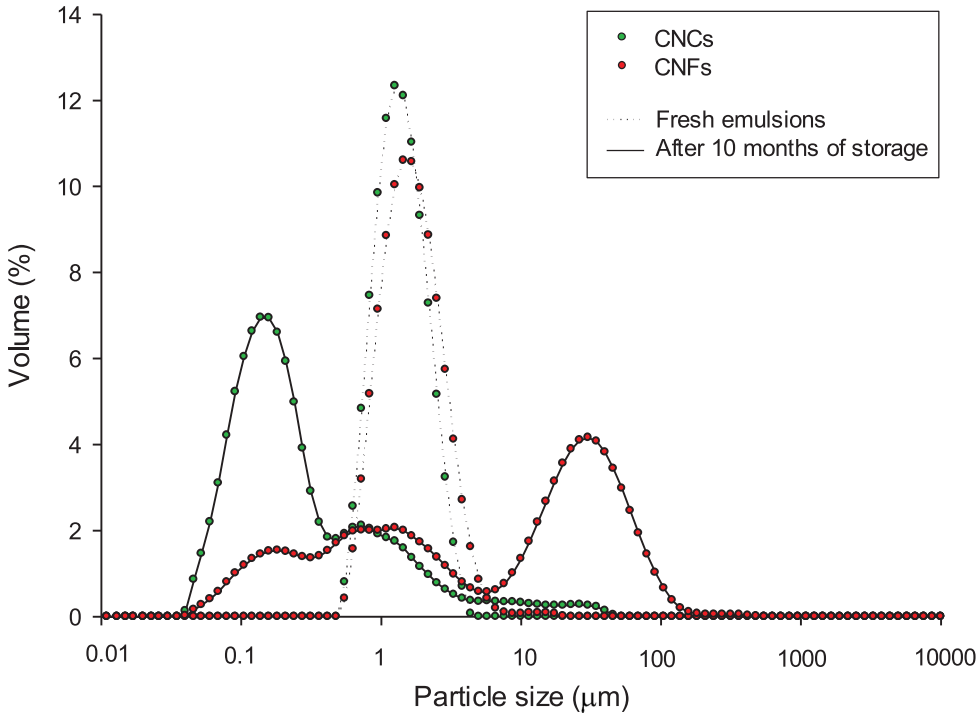

Figure 12. Droplet size distributions of CNCs and CNFs stabilized emulsions on day 0 (··· dotted line) and 10-months of storage (— solid line).

emulsion is of interest for application in in different fields. To this purpose, further studies are required for a comprehensive understanding of emulsion stabilization mechanisms.

The droplet size distribution measurements confirmed the microscopy observations, showing a decrease in droplet volume diameter for CNCs and an increase in CNFs after 10 months of storage (Figure 12). Remarkably, both CNCs- and CNFs-stabilized emulsions initially exhibited monomodal distributions, characterized by relatively small span values (1.17 and 1.40 for CNCs and CNFs, respectively) and transitioned to bimodal distributions during storage, with significantly larger span values (8.28 and 5.82 for CNCs and CNFs, respectively).

3. Conclusion

This study focuses on applying TEMPO-mediated oxidation to softwood kraft pulp Celeste 85 to obtain CNCs or CNFs, both possessing distinctive properties in terms of morphology, carboxylate group content, and wettability, are suitable for the stabilization of Pickering emulsions. These NCs are found to be suitable for stabilizing Pickering emulsions. The results show that the obtained CNCs, featuring a needle-like structure of ≈3 nm in thickness and ≈170 nm in length, and CNFs, characterized by a fibrous structure with dimensions of ≈10 nm in thickness and a few micrometers in length, effectively stabilize 5 wt% sunflower oil-based Pickering emulsions at a dosage of 0.5 wt%. Despite the significant morphological differences between CNCs and CNFs, both contribute to forming an interconnected network structure within the emulsion droplets, promoting efficient steric and electrostatic stabilization. Remarkably, when emulsions are produced via HPH, the treatment has a more pronounced effect on emulsification ability and stability on CNFs, likely attributed to a defibrillation process, enhancing CNFs performance to the level of CNCs. These results provide specific insights into how tailoring the properties of nanostructured cellulose during fabrication, through TEMPO-mediated oxidation and HPH, can be a straightforward strategy to influence the behavior and stability of Pickering emulsions. Specifically, CNCs can be employed in the stabilization of emulsions for low-viscosity applications, such as drinks and beverages, owing to the finer attainable emulsion size and span values. On the other hand, CNFs could find application in creams, sauces and dressings, benefiting from their higher apparent viscosity and the robust 3D-network formed by entangled fibers.

4. Experimental Section

Materials: Northern bleached softwood kraft pulp (Celeste 85) was a kind gift of SCA (Sundsvall, Sweden). This pulp was manufactured through a totally chlorine-free thermomechanical process and flush-dried.

Peanut oil, purchased from a local market (Olio di Semi di Arachide Giglio Oro, Firenze, Italy), was used as the oil phase in the experiment. According to the manufacturer's specifications, its composition on weight basis, comprises 18 wt% of saturated fatty acids, 46 wt% of monounsaturated fatty acids, and 28 wt% of polyunsaturated fatty acids.

Sodium dodecyl sulfate ($C_{12}H_{25}NaO_4S$, ACS GR, 99.0%, PanReac, Barcelona, Spain) was used as received without further purification. Milli-Q water (obtained with Barnstead Pacific TII Water, Thermo Scientific, Waltham, MA, USA) was used throughout the course of this study.

Preparation of NCs: TEMPO-mediated oxidation of cellulose pulp was conducted following the method of Saito and Isogai (Saito & Isogai, 2004), with slight modifications, as herein reported. To obtain CNCs, 5 g of Celeste 85 pulp were swollen in 400 mL H_2O. Subsequently, a solution containing 83 mg of 2,2,6,6-Tetramethylpiperidine-1oxyl (TEMPO, $C_9H_{19}N$, ≥98.0%, Alfa Aesar Chemicals, Ward Hill MA, USA), the reaction catalyst, and 0.5 g of sodium bromide (NaBr, ≥99.99%, Carlo Erba, Milan, Italy), the catalyst re-cycling, in 100 mL H_2O were added to the pulp suspension. The reaction was started by adding 18 mL of sodium hypochlorite containing 6–14% active chlorine (NaClO, Sigma–Aldrich, Milan, Italy), the primary oxidant. The pH of the reaction mixture was maintained within the interval 10.5–11 by incremental addition of NaOH until a constant pH was achieved, typically after 4 h. Subsequently, the suspension was rinsed several times with H_2O and was subjected to tip sonication at 80% power. The sonication process was carried out using a Bandelin Sonuplus ultrasonicator system (Berlin, Germany) on suspension aliquots of 35 mL volume. For the production of CNFs, the same procedure was employed, with the exception that a reduced quantity of TEMPO (12.5 mg) was used, and the reaction was terminated after 2 h.

Preparation of Pickering Emulsions: Coarse O/W emulsions were prepared by mixing peanut oil (5 wt%) with the aqueous phase (95 wt%) containing 0.5 wt% of CNCs or CNFs in ultrapure H_2O. The mixing process was carried out in a HSM (MIULab MT-30 K Handheld Homogenizer, Hangzhou, China) operating at 35 000 rpm for 5 min within an ice bath. Subsequently, the obtained coarse emulsions underwent further treatment through a HPH process at 80 MPa under recycle mode, for 15 equivalent passes, with the heat exchangers set at 5 °C. The HPH was performed using a laboratory setup, specifically an orifice-type homogenizer, as previously described in detail by Pirozzi et al.[42]

NCs Characterization: Atomic Force Microscopy (AFM) images were captured using an NT-MDT P47H probe microscope (Apeldoorn, Netherlands) scanning operated in the semi-contact mode with a tip spring constant of 40 N m^{-1}. Detailed information regarding the size and morphology of the CNCs and CNFs, produced by the TEMPO-mediated oxidation procedure, was obtained by analyzing these images with the Gwyddion 2.59 software.

Infrared spectra of CNCs and CNFs were acquired utilizing a Nicolet IN10 microFTIR instrument (Thermo Fisher Scientific, Waltham MA, USA) in transmittance mode. For this purpose, drops of CNCs' and CNFs' suspensions were deposited on ZnSe optical windows and left to dry in an oven.

The carboxylation of CNCs and CNFs was determined through conductometric titration using a Delta Ohm 2256 instrument (Padova, Italy). The samples were initially adjusted to pH 2.8 by the addition of HCl. Subsequently, the solution was titrated with 0.5 M NaOH. The degree of oxidation (OD), representing the carboxyl content per weight of CNCs and CNFs (μmol mg^{-1}), was calculated using Equation (1):

$$OD = \frac{C \cdot V}{m} \quad (1)$$

where C is the concentration of the NaOH solution, and m is the total mass of CNCs and CNFs measured after oven drying the suspensions. V is the volume of the NaOH solution added to reach complete ionization of COOH groups, which was obtained by fitting the experimental titration curve.[67]

The interfacial tensions of NCs (0.5 wt%) were determined through the pendant drop method using a contact-angle meter (KSV Instruments LTD CAM 200, Helsinki, Finland), equipped with an image analysis software. Briefly, a syringe equipped with a stainless-steel needle (0.71 mm in diameter) filled with the aqueous phase containing nanoparticles was submerged into the oil phase within a glass cuvette. Throughout the experiments, the initial volume of the formed drop was ≈30 μL. The contact angle meter recorded the dynamic change of the water–oil interface, and the Young–Laplace equation was subsequently used to calculate the interfacial tension. Distilled water was used as the control in these experiments. Interfacial tension (γ) measurements were performed over a pe-

riod of 2500 s, and equilibrium interfacial tension values were estimated using the exponential decay model of Equation (2)[68]:

$$\gamma = \gamma_\infty + (\gamma_0 - \gamma_\infty)\, e^{-\frac{t}{\tau_r}} \tag{2}$$

where γ_∞ is the asymptotic interfacial tension, γ_0 is the initial interfacial tension, τ_r is the characteristic time for the arrangement of the molecules at the water–oil interface, and t is the time variable.

The ζ-potential of the cellulose nanoparticles in water was measured by dynamic light scattering (DLS) and electrophoretic mobility using a Zetasizer Nano (ZEN3600 Malvern Instruments Ltd., Malvern, UK) at 25 °C.

Pickering Emulsions Characterization: The microscopic structure of Pickering emulsions prepared with CNCs and CNFs was observed using the optical inverted microscope Nikon Eclipse (TE 2000S, Nikon instruments Europe B.V., Amsterdam, The Netherlands).

The emulsions size distributions were measured via laser diffraction using a Mastersizer 2000 instrument (Malvern instrument Ltd., Malvern, UK), applying the Fraunhofer approximation, which does not require prior knowledge of the optical properties of the sample. The temperature of the cell was maintained at 25 ± 0.5 °C throughout the measurements. Characteristic diameters d(0.1), d(0.5), and d(0.9), representing 10th, 50th (median value), and 90th percentile of the cumulative size distribution of the suspensions, were determined. Additionally, the surface-weighted mean diameter D[3,2] and volume-weighted mean diameter D[4,3] were calculated according to Equations (3) and (4), respectively:

$$D\ [3,2] = \frac{\sum_i n_i d_i^3}{\sum_i n_i d_i^2} \tag{3}$$

$$D\ [4,3] = \frac{\sum_i n_i d_i^4}{\sum_i n_i d_i^3} \tag{4}$$

where n_i is the number of particles of diameter d_i.

The relative span factors were calculated according to Equation (5), to express the distribution width of the droplet size distribution:

$$Span = \frac{d\,(0.9) - d\,(0.1)}{d\,(0.5)} \tag{5}$$

The surface coverage (SC) of NCs of the internal phase of the Pickering emulsions was given by the ratio of the theoretical maximum surface area by the particles (S_P) to the total surface displayed by the oil droplets (S_d), as per Equation (6)[69–71]:

$$SC = \frac{S_P}{S_d} = \frac{m_P \cdot D\,[3,2]}{6 \cdot h \cdot \rho_P \cdot V} \tag{6}$$

where m_P represents the mass of NCs in the Pickering emulsion (g), D[3,2] is the surface-weighted mean diameter, h is the thickness of cellulose fibers (average thickness of CNCs and CNFs fibers is 3.0 ± 0.5 and 10 nm, respectively, as estimated through AFM), ρ_P is the cellulose density (1.6 g cm^{-3}), and V is the volume of oil used in the Pickering emulsion (mL).

The rheological properties of Pickering emulsions were characterized using a rotational rheometer (AR 2000 rheometer, TA instruments, Newcastle, DE, USA), equipped with a concentric cylinder (15 mm stator inner diameter, 28 mm rotor outer diameter, 42 mm cylinder immersed height, 2° cone angle). Viscosity curves were obtained by varying the shear rate from 0.1 s^{-1} up to 200 s^{-1}, with the temperature maintained at 20 °C.

The stability of the emulsions was determined using the turbidimetric method.[72] Absorbance values of freshly prepared emulsions (t_0) and after 30 min (t_{30}) were recorded at 500 nm against a blank (dilution solution), following the introduction of 50 µL of emulsion into 5 mL of 0.1 wt% sodium dodecyl sulfate (SDS) solution. Turbidity (T) was calculated using Equation 7:

$$T = 2.303 \cdot \frac{A \cdot DF}{OP} \tag{7}$$

where A is the absorbance of the sample at t_0 and 500 nm, DF is the dilution factor, and OP is the optical path (1 cm, in the used equipment).

The emulsifying activity index (EAI) and the emulsion stability index (ESI) were calculated using Equations (8) and (9), respectively.

$$EAI\ \left(\frac{m^2}{g}\right) = 2 \cdot \frac{T}{(1-\vartheta) \cdot C \cdot 1000} \tag{8}$$

$$ESI\ (-) = \frac{EAI_{t_0}}{EAI_{t_0} - EAI_{t_{30}}} \cdot 100 \tag{9}$$

where T is the turbidity, ϑ is the volume fraction of oil in the emulsion, and C (g mL^{-1}) is the initial concentration of NCs. EAI_{t0} and EAI_{t30} are the emulsifying activity indexes calculated at 0 and 30 min, respectively.

Statistical Analysis: The experiments were conducted in triplicates, and the resulting values are presented as mean ± standard deviation. Statistical analysis was performed to identify significant differences, with a significance level set at $p < 0.05$. The analysis was carried out using the SPSS 20 statistical package (SPSS Inc., Chicago, IL, USA). The one-way analysis of variance (ANOVA) was employed to assess overall differences among groups, followed by Tukey's test for post-hoc analysis. It is noteworthy that the data exhibited a normal distribution, validating the appropriateness of the selected statistical tests.

Acknowledgements

This study received funding from the MIUR under the project PRIN PANACEA (2017LEPH3M); CUP D44I17000230006.

Open Access Funding provided by Ministero dell'Istruzione, dell'Universitá e della Ricerca within the CRUI-CARE Agreement.

Conflict of Interest

The authors declare no conflict of interest.

Data Availability Statement

The data that support the findings of this study are available from the corresponding author upon reasonable request.

Keywords

emulsifying property, emulsion stability, high-pressure homogenization, nanocellulose, TEMPO oxidation

Received: December 20, 2023
Revised: February 5, 2024
Published online: March 3, 2024

[1] H. Xiong, X. Xie, Y. Li, L. Li, *Colloids Surfaces A Physicochem. Eng. Asp.* **2023**, *673*, 131797.
[2] B. Ding, S. H. Ahmadi, P. Babak, S. L. Bryant, A. Kantzas, *Langmuir* **2023**, *39*, 6975.

[3] J. Wu, G.-H. Ma, *Small* **2016**, *12*, 4633.
[4] Z. Li, D. Yu, *Int. J. Biol. Macromol.* **2023**, *242*, 124942.
[5] Y. Li, D. Yu, X. Wang, Q. Wang, Z. Zhang, W. Liu, *Cellulose* **2022**, *29*, 3253.
[6] N. Nimaming, A. Sadeghpour, B. S. Murray, A. Sarkar, *Trends Food Sci. Technol.* **2023**, *138*, 671.
[7] A. De Bruno, R. Romeo, A. Piscopo, M. Poiana, *J. Sci. Food Agric.* **2020**, *101*, 3535.
[8] S. Zhang, W. Jiang, Z. Zhang, Y. Zhu, L. Wang, J. Fu, *LWT – Food Sci. Technol.* **2020**, *130*, 109369.
[9] Z. Wang, D. Yu, *Cellulose* **2023**, *30*, 9607.
[10] D. Yu, Q. Luo, J. Zhang, Q. Wang, H. Wang, Z. Song, S. Li, W. Liu, F. Zhang, D. Ji, *Cellulose* **2022**, *29*, 8569.
[11] I. Shabir, A. Hussain, K. Kumar, S. Srivastava, V. Kumar, S. Manzoor, S. Manzoor, I. Bashir, *J. Agric. Food Res.* **2023**, *14*, 100853.
[12] Y. Yang, Z. Fang, X. Chen, W. Zhang, Y. Xie, Y. Chen, Z. Liu, W. Yuan, *Front Pharmacol.* **2017**, *8*, 287.
[13] K. J. M. Bishop, C. E. Wilmer, S. Soh, B. A. Grzybowski, *Small* **2009**, *5*, 1600.
[14] H. M. Kipen, D. L. Laskin, *Am. J. Physiol. Lung Cell Mol. Physiol.* **2005**, *289*, L696.
[15] H. Dupont, V. Maingret, V. Schmitt, V. Héroguez, *Macromolecules* **2021**, *54*, 4945.
[16] Y. Xue, Z. Mou, H. Xiao, *Nanoscale* **2017**, *9*, 14758.
[17] S. Meschini, E. Pellegrini, C. A. Maestri, M. Condello, P. Bettotti, G. Condello, M. Scarpa, *J. Biomed. Mater. Res.* **2020**, *108*, 687.
[18] K. J. De France, T. Hoare, E. D. Cranston, *Chem. Mater.* **2017**, *29*, 4609.
[19] C. Jiménez Saelices, I. Capron, *Biomacromolecules* **2018**, *19*, 460.
[20] Y. Habibi, *Chem. Soc. Rev.* **2014**, *43*, 1519.
[21] C. A. Maestri, M. Abrami, S. Hazan, E. Chistè, Y. Golan, J. Rohrer, A. Bernkop-Schnürch, M. Grassi, M. Scarpa, P. Bettotti, *Sci. Rep.* **2017**, *7*, 11129.
[22] H. Voisin, X. Falourd, C. Rivard, I. Capron, *JCIS Open* **2021**, *3*, 100014.
[23] A. Pirozzi, E. Rincón, E. Espinosa, F. Donsì, L. Serrano, *Gels* **2023**, *9*, 958.
[24] W. Qu, Z. Wang, M. Qin, X. Yang, F. Zhang, Z. Wang, D. Ji, D. Yu, *Sep. Purif. Technol.* **2023**, *325*, 124673.
[25] F. Jiang, Y. Lo Hsieh, *ACS Sustainable Chem. Eng.* **2016**, *4*, 1041.
[26] S. H. Teo, C. Y. Chee, M. Z. Fahmi, S. C. W. Sakti, H. V. Lee, *Molecules* **2022**, *27*, 7170.
[27] B. Medronho, B. Lindman, *Curr. Opin. Colloid Interface Sci.* **2014**, *19*, 32.
[28] A. Pirozzi, A. Posocco, F. Donsì, *Food Hydrocoll* **2023**, *145*, 109152.
[29] H. Kargarzadeh, M. Ioelovich, I. Ahmad, S. Thomas, A. Dufresne, in Handb. Nanocellulose Cellul. Nanocomposites, **2017**.
[30] A. Isogai, T. Saito, H. Fukuzumi, *Nanoscale* **2011**, *3*, 71.
[31] T. Thi Thanh Hop, D. Thi Mai, T. Duc Cong, T. T. Y. Nhi, V. Duc Loi, N. Thi Mai Huong, N. Trinh Tung, *Results Chem.* **2022**, *4*, 100540.
[32] H. Xu, J. L. Sanchez-Salvador, A. Blanco, A. Balea, C. Negro, *Carbohydr. Polym.* **2023**, *319*, 121168.
[33] H. Xu, J. L. Sanchez-Salvador, A. Balea, A. Blanco, C. Negro, *Cellulose* **2022**, *29*, 6611.
[34] M. Rajinipriya, M. Nagalakshmaiah, M. Robert, S. Elkoun, *ACS Sustainable Chem. Eng.* **2018**, *6*, 2807.
[35] T. Benselfelt, N. Kummer, M. Nordenström, A. B. Fall, G. Nyström, L. Wågberg, *ChemSusChem* **2023**, *16*, 1.
[36] A. Shinsho, T. Brenner, F. B. Descallar, Y. Tashiro, N. Ando, Y. Zhou, H. Ogawa, S. Matsukawa, *Food Hydrocoll* **2020**, *109*, 105997.
[37] S. Fujisawa, R. Tanaka, Y. Hayashi, Y. Yabuhara, M. Kume, T. Saito, *Polym. J.* **2023**, *55*, 223.
[38] F. Ravera, K. Dziza, E. Santini, L. Cristofolini, L. Liggieri, *Adv. Colloid Interface Sci.* **2021**, *288*, 102344.
[39] Y. Ni, J. Li, L. Fan, *Int. J. Biol. Macromol.* **2020**, *149*, 617.
[40] Y. Goi, S. Fujisawa, T. Saito, K. Yamane, K. Kuroda, A. Isogai, *Langmuir* **2019**, *35*, 10920.
[41] S. Parajuli, E. E. Ureña-Benavides, *Adv. Colloid Interface Sci.* **2022**, *299*, 102530.
[42] A. Pirozzi, R. Capuano, R. Avolio, G. Gentile, G. Ferrari, F. Donsì, *Foods* **2021**, *10*, 1886.
[43] E. J. Foster, R. J. Moon, U. P. Agarwal, M. J. Bortner, J. Bras, S. Camarero-Espinosa, K. J. Chan, M. J. D. Clift, E. D. Cranston, S. J. Eichhorn, D. M. Fox, W. Y. Hamad, L. Heux, B. Jean, M. Korey, W. Nieh, K. J. Ong, M. S. Reid, S. Renneckar, R. Roberts, J. A. Shatkin, J. Simonsen, K. Stinson-Bagby, N. Wanasekara, J. Youngblood, *Chem. Soc. Rev.* **2018**, *47*, 2609.
[44] R. J. Hunter, *Acad. Press* **2013**.
[45] T. Rosén, H. R. He, R. Wang, C. Zhan, S. Chodankar, A. Fall, C. Aulin, P. T. Larsson, T. Lindström, B. S. Hsiao, *ACS Nano* **2020**, *14*, 16743.
[46] L. Solhi, V. Guccini, K. Heise, I. Solala, E. Niinivaara, W. Xu, K. Mihhels, M. Kröger, Z. Meng, J. Wohlert, H. Tao, E. D. Cranston, E. Kontturi, *Chem. Rev.* **2023**, *123*, 1925.
[47] S. A. Kedzior, V. A. Gabriel, M. A. Dubé, E. D. Cranston, *Adv. Mater.* **2021**, *33*, https://doi.org/10.1002/adma.202002404.
[48] N. Rehman, H. Ullah, S. Alam, A. K. Jan, S. W. Khan, M. Tariq, *J. Mater. Environ. Sci.* **2017**, *8*, 1161.
[49] W. Liang, F. Deng, Y. Wang, W. Yue, D. Hu, J. Rong, R. Liu, S. Xiong, Y. Hu, *Food Hydrocoll* **2024**, *149*, 109611.
[50] A. Pirozzi, F. Donsì, *Molecules* **2023**, *28*, 5657.
[51] S. Gharehkhani, E. Sadeghinezhad, S. N. Kazi, H. Yarmand, A. Badarudin, M. R. Safaei, M. N. M. Zubir, *Carbohydr. Polym.* **2015**, *115*, 785.
[52] P. Bertsch, P. Fischer, *Adv. Colloid Interface Sci.* **2020**, *276*, 102089.
[53] L. S. Martins, R. G. dos Santos, M. A. S. Spinacé, *Waste Biomass Valorization* **2022**, *13*, 689.
[54] R. Pal, *AIChE J.* **1996**, *42*, 3181.
[55] I. Kalashnikova, H. Bizot, P. Bertoncini, B. Cathala, I. Capron, *Soft Matter* **2013**, *9*, 952.
[56] H. Dong, Q. Ding, Y. Jiang, X. Li, W. Han, *Carbohydr. Polym.* **2021**, *265*, 118101.
[57] T. Tang, *Nonlinear Anal.: Real World Appl.* **2020**, *56*, 103172.
[58] S. Varanasi, L. Henzel, L. Mendoza, R. Prathapan, W. Batchelor, R. Tabor, G. Garnier, *Front Chem.* **2018**, *6*, 409.
[59] H. Yang, Z. Su, X. Meng, X. Zhang, J. F. Kennedy, B. Liu, *Carbohydr. Polym.* **2020**, *247*, 116712.
[60] A. L. R. Costa, A. Gomes, L. B. Cangussu, R. L. Cunha, L. S. de Oliveira, A. S. Franca, *Food Res. Int.* **2022**, *152*, 110930.
[61] M. S. Reid, M. Villalobos, E. D. Cranston, *Nanoscale* **2016**, *8*, 12247.
[62] T. Yuan, J. Zeng, B. Wang, Z. Cheng, K. Chen, *Carbohydr. Polym.* **2021**, *269*, 118339.
[63] X. Bao, X. Yan, G. Zhang, J. Zhao, Z. Zeng, P. Yu, D. Gong, *Lwt* **2022**, *155*, 112948.
[64] Y. Liu, Y. P. Xie, X. Y. Ma, L. N. Liu, Y. J. Ke, *J. Food Meas. Charact.* **2022**, *16*, 410.
[65] L. Bai, S. Lv, W. Xiang, S. Huan, D. J. McClements, O. J. Rojas, *Food Hydrocoll* **2019**, *96*, 699.
[66] J. Ojala, M. Visanko, O. Laitinen, M. Österberg, J. A. Sirviö, H. Liimatainen, *Molecules* **2018**, *23*, 2765.
[67] D. Da, S. Perez, S. Montanari, M. R. Vignon, *Biomacromolecules* **2003**, *4*, 1417.
[68] E. Mauriello, G. Ferrari, F. Donsì, *Colloids Surf., B* **2021**, *197*, 111424.
[69] K. He, X. Zhang, Y. Li, B. Li, S. Liu, *Food Hydrocoll* **2020**, *101*, 105519.
[70] Z. Hu, T. Patten, R. Pelton, E. D. Cranston, *ACS Sustainable Chem. Eng.* **2015**, *3*, 1023.
[71] I. Kalashnikova, H. Bizot, B. Cathala, I. Capron, *Langmuir* **2011**, *27*, 7471.
[72] S. De Maria, G. Ferrari, P. Maresca, *Innov. Food Sci. Emerg. Technol.* **2016**, *33*, 67.

